**Abstract**

# Measurement of total hadronic differential cross sections in the LArIAT experiment

Elena Gramellini

2018

Abstract goes here. Limit 750 words.

# Measurement of total hadronic differential cross sections in the LArIAT experiment

A Dissertation
Presented to the Faculty of the Graduate School
of
Yale University
in Candidacy for the Degree of
Doctor of Philosophy

by
Elena Gramellini

Dissertation Director: Bonnie T. Fleming

Date you'll receive your degree

# Contents

# Acknowledgements

A lot of people are awesome, especially you, since you probably agreed to read this when it was a draft.

# Chapter 0

# Samples Preparation

This chapter describes the preparation of the data and Monte Carlo samples used for the cross section analyses. This entails:

1. the beamline event selection on data,
2. the MC production,
3. the energy calibration of the detector both in data and MC,
4. the optimization of the tracking algorithm for the total cross section analyses.

## 0.1 LArIAT Data

## 0.2 LArIAT Monte Carlo

For the simulation of LArIAT events and their particle make up, we use a combination of two MC generators: the G4Beamline Monte Carlo and the Data Driven single particle Monte Carlo (DDMC). We use the G4Beamline MC to simulate the particle transportation in the beamline and calculate the particle composition of the beam just past the fourth Wire Chamber (WC4). In order to simulate the beam line particles after WC4 and in the TPC, we use the DDMC.

### 0.2.1 G4Beamline

G4Beamline simulates the beam collision with the LArIAT secondary target, the energy deposited by the particles in the LArIAT beamline detectors and the action of the LArIAT magnets, effectively accounting for particle transportation through the beam line from the LArIAT target until "Big Disk", a fictional, void detector located just before the cryostat. At the moment of this writing, G4Beamline does not simulated the responses of the beam line detectors. It is possible to interrogate the truth level information of the simulated particles in several points of the geometry. In order to ease the handshake between G4Beamline and the DDMC, we ask for the beam composition just after WC4. Since LArIAT data are taken under different beam conditions, G4Beamline simulates separately the beam composition according to the magnets' settings and the secondary beam intensity. For the pion cross section analysis the relevant beam conditions are secondary beam energy of 64 GeV, negative polarity magnet with current of 100 A and 60 A. For the kaon cross section analysis the relevant beam conditions is a secondary beam energy of 64 GeV, positive polarity magnet with current of 100 A.

DECIDE IF YOU WANT THE BEAM COMPOSITION HERE

### 0.2.2 Data Driven MC

The Data Driven single particle Monte Carlo (DDMC) is a single particle MC gun which simulates the particle transportation from WC4 into the TPC leveraging on the beamline data information. The DDMC uses the data momentum and position at WC4 to derive its initial conditions: a general sketch of the DDMC workflow is shown in Figure 1.

When producing a DDMC sample, beam line data from a particular running period and/or running condition are selected first. Figure 2 schematically shows the data quantities of interest leveraged from data: the momentum $(P_x, P_y, P_z)$ and position $(X, Y)$ at WC4. For each data event, we obtain the particle position $(X, Y)$ at WC4 directly from the data measurement. On the contrary, we calculate the components of the momentum using the beamline measurement of the momentum magnitude (see section **??**) in conjunction with the hits on WC3 and WC4 to determine the direction of the momentum vector. The momentum and position of the selected data is sampled thousand of times through a 5-dimensional hit-or-miss sampling procedure. This produces MC distributions with the same momentum and position distributions as data, with the additional benefit of accounting for the correlations between the considered variables. A LArSoft simulation module then launches single particle MC from z = -100 cm (the location of the WC4) using the sampled momentum and position distributions as a template. An illustration of this procedure is shown in Figure 17 with the results of the DDMC generation compared to a sample of wire chamber track data. Using this technique ensures the MC and data have very similar momentum, position and angular distributions at Wire-Chamber 4 and allow us to calibrate the energy loss upstream of the TPC as precisely as possible. The DDMC is a single particle Monte Carlo: the beam pile-up is not simulated. A sample of NUMBERS pions and NUMBERS kaons have been generated with the DDMC and used for the MC cross section study.

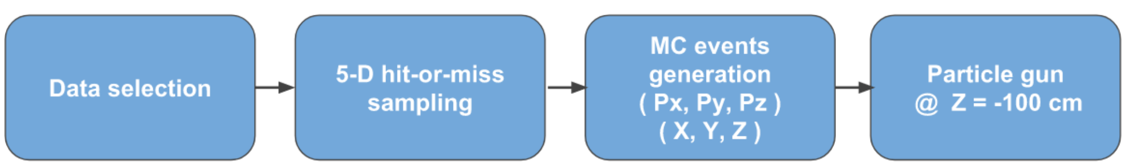


Figure 1: Workflow for Data Driven single particle Monte Carlo production.

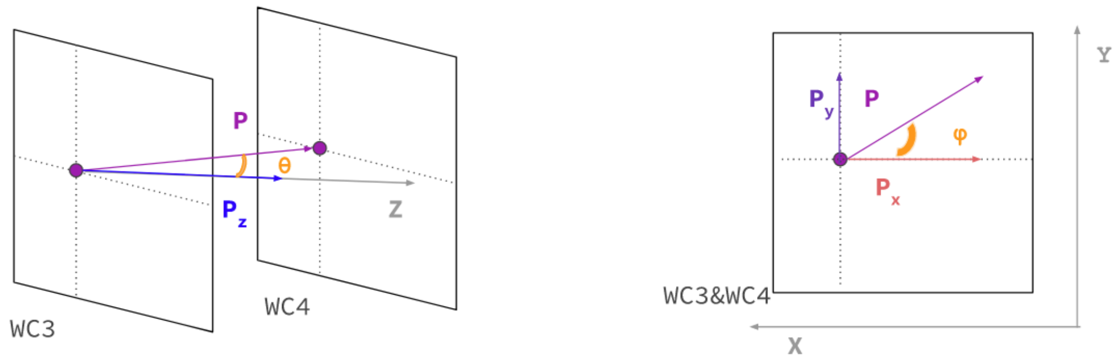


Figure 2: Scheme of the quantities of interest for the DDMC event generation: $P_x, P_y, P_z, X, Y$ at WC4.

## 0.3 Energy Calibration

## 0.4 Tracking Studies

In this section, we describe three studies. The first is a justification of the selection criteria for the beamline handshake with the TPC information. We perform this study to boost the correct identification of the particles in the TPC associated with the beamline information, while maintaining sufficient statistics for the cross section measurement. The second study is an optimization of the tracking algorithm, with the scope of maximizing the identification of the hadronic interaction point inside the TPC. These two studies are related, since the optimization of the tracking is performed on TPC tracks which have been matched to the wire chamber track; in turn, the tracking algorithm for TPC tracks determine the number of reconstructed tracks in each event used to try the matching with the wire chamber track. Starting with a sensible tracking reconstruction, we perform the WC2TPC matching optimization first, then the tracking optimization. The WC2TPC match purity and efficiency are then calculated again with the optimized tracking.

We perform the following studies on a MC sample of 191000 kaons and 359000 pions produced with the DDMC technique. DDMC particles are shot from the WC4 location into the TPC following the beam profile. We mimic the matching between the WC and the TPC track on Monte Carlo by constructing a fake WC track using truth information at wire chamber four. We then apply the same WC to TPC matching algorithm as in data described in **??**.

### 0.4.1 Selection Study for the Wire Chamber to TPC Match

Plots I want in this section:

1. WC2TPC MC DeltaX, DeltaY and $\alpha$

Scope of this study is assessing the goodness of the wire chamber to TPC match on Monte Carlo and decide the selection values we will use on data. A word of caution is necessary here. With this study, we want to minimize pathologies associated with the presence of the primary hadron itself, e.g. the incorrect association between the beamline hadron and its decay products inside the TPC. Assessing the contamination from pile-up[1], albeit related, is beyond the scope of this study.

In MC, we are able to define a correct WC2TPC match using the Geant4 truth information. We are thus able to count how many times the WC tracks is associated with the wrong TPC reconstructed track.

We define a correct match if the all following conditions are met:

- the length of the true primary Geant4 track in the TPC is greater than 2 cm,
- the length of the reconstructed track length is greater than 2 cm,
- the Z position of the first reconstructed point is within 2 cm from the TPC front face

1. We remind the reader that the DDMC is a single particle Monte Carlo, where the beam pile up is not simulated.

- the distance between the reconstructed track and the true entering point is the minimum compared with all the other reconstructed tracks.

In order to count the wrong matches, we consider all the reconstructed tracks whose Z position of the first reconstructed point lies within 2 cm from the TPC front face. Events with true length in TPC $< 2$ cm are included. Since hadrons are shot 100 cm upstream from the TPC front face, the following two scenarios are possible from a truth standpoint:

[$Ta$ ] the primary hadron decays or interact strongly before getting to the TPC,

[$Tb$ ] the primary hadron enters the TPC.

Once we choose the selection cuts to determine a reconstructed wire chamber-to-TPC match $r_T$ and $\alpha_T$, the following five scenarios are possible in the truth to reconstruction interplay :

1) only the correct track is matched

2) only one wrong track is matched

3) the correct track and one (or more) wrong tracks are matched

4) multiple wrong tracks matched.

5) no reconstructed tracks are matched

Since we keep only events with one and only one match, we discard cases 3), 4) and 5) from the events used in the cross section measurement. For each set of $r_T$ and $\alpha_T$ selection value, we define purity and efficiency of the selection as follows:

$$\text{Efficiency} = \frac{\text{Number of events correctly matched}}{\text{Number of events with primary in TPC}} \tag{1}$$

$$\text{Purity} = \frac{\text{Number of events correctly matched}}{\text{Total number of matched events}}. \tag{2}$$

Figure 3 shows the efficiency (left) and purity (right) for wire chamber-to-TPC match as a function of the radius, $r_T$, and angle, $\alpha_T$, selection value. It is apparent how both efficiency and purity are fairly flat as a function of the radius selection value at a given angle. This is not surprising. Since we are studying a single particle gun Monte Carlo sample, the wrong matches can occur only for mis-tracking of the primary or for association with decay products; decay products will tend to be produced at large angles compared to the primary, but could be fairly close to the in $x$ and $y$ projection of the primary. The radius cut would play a key role in removing pile up events.

For LArIAT cross section measurements, we generally prefer purity over efficiency, since a sample of particles of a pure species will lead to a better measurement. Obviously, purity should be balanced with a sensible efficiency to avoid rejecting the whole sample.

We choose $(\alpha_T, r_T) = (8\text{ deg}, 4\text{ cm})$ and get a MC 85% efficiency and 98% purity for the kaon sample and a MC BOH% efficiency and 98% purity for the BOH sample.

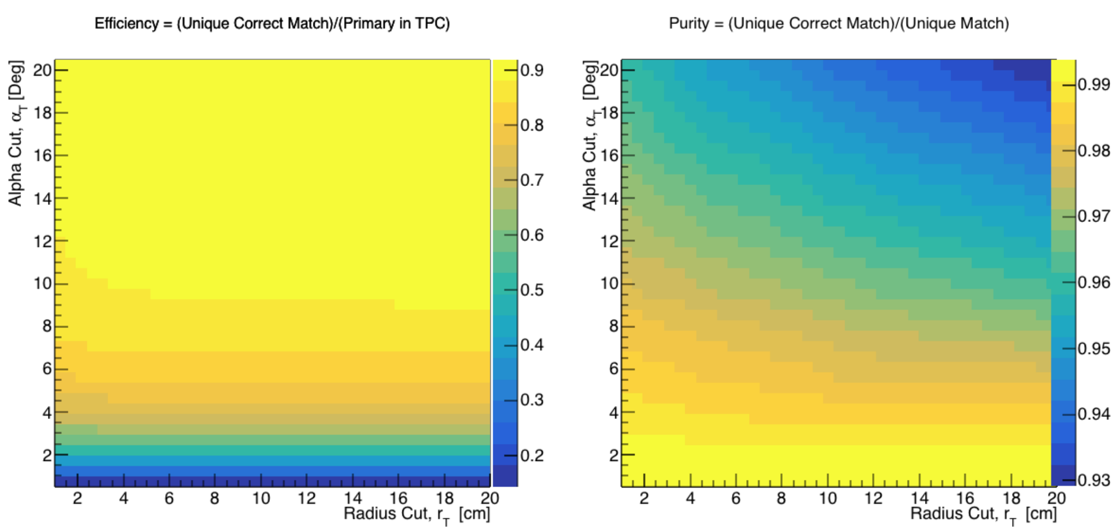


Figure 3: Efficiency (left) and purity (right) for wire chamber-to-TPC match as a function of the radius and angle selections.

### 0.4.2 Interaction Point Optimization

Scheme of this subsection

**Brief Explanation of the reconstruction chain**

**Explanation of clustering parameters**

**Figure of merit and spanning of cluster**

**Important numbers out of this optimization**

Plots I want in this section:

1. Delta L, reco - true
2. Delta L, reco - true Elastic, Delta L, reco - true Inelastic, other
3. Length Quality cut
4. Efficiency as a function of true KE and Angle

### 0.4.3 Tracking spatial and angular resolution

Scope of this study is understanding and comparing the tracking spatial and angular resolution on data and MC. We start by selecting all the WC2TPC matched tracks. We fit a line on all the space points of the track and calculate the $\chi^2$. The $\chi^2$ distribution for data and MC is shown in Figure **??**.

For the spatial and angular resolution study, we reject tracks with less than 14 space points. For each track, we order the space points according to their Z position and we split them in two sets: the first set counts all the points belonging to the first half of the track and the second set counts all the points belonging to the second half of the track. We remove the last 5 points in the first set and the first 5 points in the second set, so to have a gap in the middle of the original track. We fit the first and the second set of points with a line separately. We reject the event entirely if the $\chi^2$ for the fit of either of the halves is greater than four. We define a track middle plane as the plane perpendicular to the original track fit, positioned in the middle of its length. We project the tracks on the middle plane and calculate the impact parameter, $d$, i.e. the distance between the projected points. We also calculate the angle between the original track direction and the fit of the first and second half, called $\alpha_1$ and $\alpha_2$ respectively. The spatial resolution of the track will be $\sigma_S = \frac{d}{\sqrt{2}}$ while the angular resolution of the tracks will be $\sigma_\alpha = \alpha_1 - \alpha_2$. The distributions for data and MC for $\sigma_\alpha$ and $\sigma_S$ are given in **??**.

### 0.4.4 Estimate of $E_{loss}$ before the TPC

The beamline particles travel a path from when their momentum is measured by the beamline detector, until they are tracked inside the TPC. In the current LArIAT geometry, a particle leaving the fourth wire chamber will encounter the materials listed in Table 1 before being registered again. The energy lost by the particle in this non instrumented material modifies the particle's kinetic energy and directly affects the cross section measurement, as shown in equation **??**.

| Material | density [g/cm$^3$] | width [cm] |
|---|---|---|
| Fiberglass laminate (G10) | 1.7 | 1.28 |
| Liquid Argon | 1.4 | 3.72 |
| Stainless Steel | 7.7 | 0.23 |
| Titanium | 4.5 | 0.04 |
| Air | $1.2 \cdot 10^{-3}$ | 89.43 |
| Plastic Scintillator | 1.03 | 5.30 |

Table 1: LArIAT material budget from WC4 to the TPC Front Face.

We estimate the uncertainty on the energy loss between the beamline momentum measurement and the TPC, $E_{loss}$, using the DDMC pion sample. We shoot pions from WC4 with the same momentum distribution as in the beamline data and plot the true $E_{loss}$ for that sample. The distribution for $E_{loss}$ for the pion sample is shown in Figure 4. We estimate the energy loss for pions to be $E_{loss} = 37 \pm 7$ MeV where we use the average energy lost as the central value and the standard deviation of the distribution as the uncertainty.

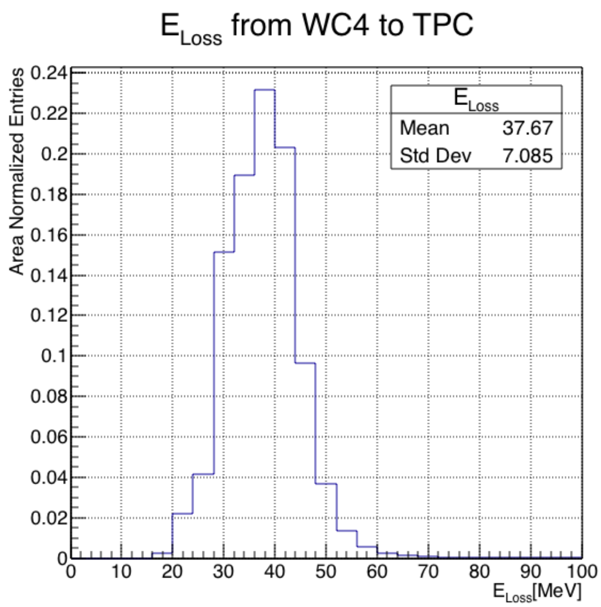


Figure 4: Energy loss by simulated negative pions downstream from WC4 and upstream from the TPC.

# Chapter 1

# Background subtraction

## 1.1 Assessing Beamline Contamination

Even if pions are by far the biggest beam component in negative polarity runs, the LArIAT beam is not a pure pion beam. While useful to discriminate between pions, kaons, and protons, the beamline detectors are not sensitive enough to discriminate among the lighter particles in the beam: electrons, muons and pions fall under the same mass hypothesis. Thus, we need to assess the contamination from beamline particles other than pions in the event selections used for the pion cross section analysis and correct for its effects.

We define beamline contamination every TPC track matched to the WC track which is not a primary pion. Potentially, there are 4 different types of beamline contaminations:

1) electrons,

2) muons,

3) secondaries from pion events,

4) matched pile up events.

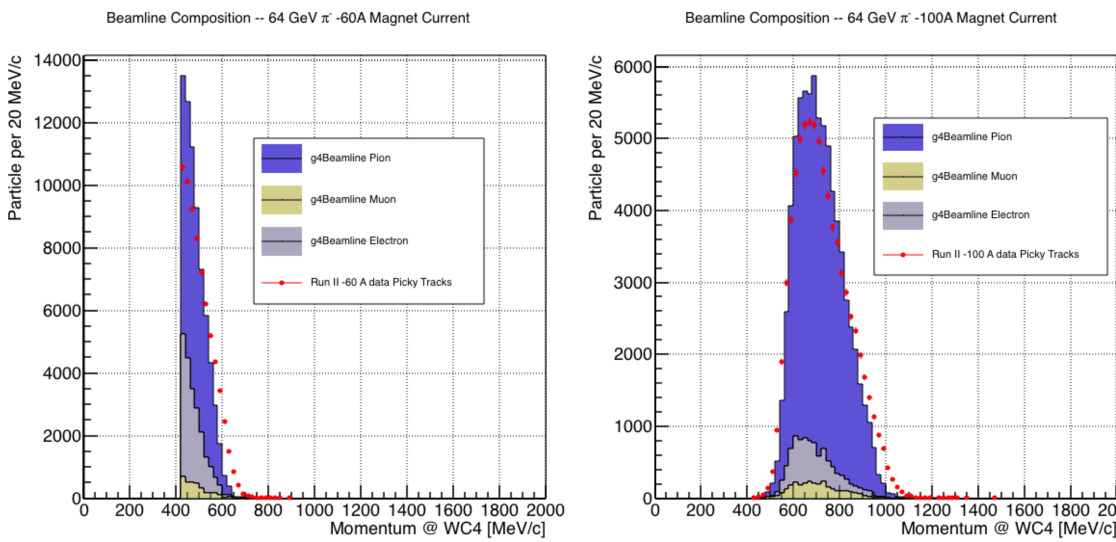


Figure 1.1: Beam composition for the -60A runs (left) and -100A runs (right). The solid blue plot represents the simulated pion content, the yellow plot represents the simulated muon content and the grey plot represents the simulated electron content. The plots are area normalized to the number of data events, shown in red.

So, how do we handle this contamination? The first step is to estimate what percentage of events used in the cross section calculation is not a primary pion. The next two sections will illustrate this estimate for the electrons, muons and secondaries from pion event. We estimate the last type of contamination, the "matched pile up" events, to be a negligible fraction, because of the definition of the WC2TPC match: we deem the probability of a single match with a halo particle in the absence of a beamline particle[1] negligibly small.

### 1.1.1 Electron and Muon contamination

We estimate the percentage of electrons and muons in the beam via the beamline MC. Since the beamline composition is a function of the magnet settings, we simulate separately events for magnet current of -60A and -100A.

Table 1.1 shows the beam composition per magnet setting after the mass selection

1. Events with multiple WC2TPC matches are always rejected.

| | I = -60 A | I = -100 A |
|---|---|---|
| G4Pions | 68.8 % | 87.4 % |
| G4Muons | 4.6 % | 3.7 % |
| G4Electrons | 26.6 % | 8.9 % |

Table 1.1: Simulated beamline composition per magnet settings

| | I = -60 A | I = -100 A | Total | $w_{60A}$ | $w_{100A}$ |
|---|---|---|---|---|---|
| N Data Events after Mass Selection | 70192 | 76056 | 146248 | 0.48 | 0.52 |

Table 1.2: Number of data events which fit the pion mass hypothesis as a function of magnet settings. The last two columns represent the faction of the data in the given magnet setting.

according to the G4Beamline simulation.

We calculate the electron to pion, as well as the muon to pion ratio on the whole sample as the weighted sum of the corresponding ratio in the two current settings,

$$\frac{N_e}{N_\pi}_{Data} = w_{60A}\frac{N_e}{N_\pi}_{60A} + w_{100A}\frac{N_e}{N_\pi}_{100A}, \tag{1.1}$$

$$\frac{N_\mu}{N_\pi}_{Data} = w_{60A}\frac{N_\mu}{N_\pi}_{60A} + w_{100A}\frac{N_\mu}{N_\pi}_{100A}, \tag{1.2}$$

where the weights $w_{60A}$ and $w_{100A}$ are the percentage of events in the corresponding magnet configuration passing the mass selection in data, as shown in table 1.2. Figure 1.1 shows the mometum predictions from G4Beamline overlaid with data for the 60A runs (left) and for the 100A runs (right). The predictions for electrons, muons and pions have been staggered and their sum is area normalized to data. Albeit not perfect, these plots show a reasonable agreement between the momentum shapes in data and MC. We attribute the difference in shape to the lack of simulation of the WC efficiency in the MC which is momentum dependent and leads to enhance the number events in the center of the momentum distribution.

Once the beam composition is know, we simulate the electrons, muons and pions with the DDMC and we subject the three samples to the same selection chain

(WC2TPC match, shower filter, pile up filter). The percentage of electrons and muons surviving the selection chain weighted by the beam composition is the electron and muon contamination in the pion cross section sample, as shown in Table 1.3.

### 1.1.2 Contamination from secondaries

Pions can travel the length of the LArIAT beamline and interact hadronically in the steel or in the non-instrumented argon upstream to the TPC front face. One of these products can leak into the TPC and be matched with the WC track, contribuiting to the pool of events used for the cross section calculation. We call this type of particles "secondaries" from pion events, with a terminology inspired by Geant4. We estimate the number of secondaries using the DDMC pion sample. The percentage of secondaries is given by the number of matched WC2TPC tracks whose corresponding particle is not flagged as primary by Geant4 and is not a muon, to avoid double counting with the G4Beamline estimate. The secondary to pion ratio is $X\%$ in the 60A sample and $Y\%$ in the 100A sample.

## 1.2 Beamline Background Subtraction

Once we estimate the contaminants to primary pion ratio, the next step is subtracting their collective contribution from data. To do so, we simulate the same number of electrons, muons and pions with the DDMC separately for the two magnet settings, and we apply the same selection filters on the three samples. The number of events per particle species surviving this selection is shown on table 1.3.

We then produce the interacting and incident histograms for the events surviving the selection for both the pions and the contaminants, weighted by the estimated beam composition.

We then evaluate the relative contribution of the contaminants bin by bin in the

| | $\pi^-$ 60A | $\mu^-$ 60A | $e^-$ 60A | $\pi^-$ 100A | $\mu^-$ 100A | $e^-$ 100A |
|---|---|---|---|---|---|---|
| Total Initial events | 334500 | 334500 | 334500 | | | |
| After Multiplicity Rejection | 331313 | 322436 | 186261 | | | |
| After WC2TPC: Selection | 201458 | 285686 | 79109 | | | |
| Evts After Shower Rejection | 191655 | 277914 | 17477 | | | |
| Survival rate | 57% | 83% | 5% | | | |
| Beam Composition After Selection | 88.5% | 8.5% | 3% | | | |

Table 1.3: MC selection flow per particle species.

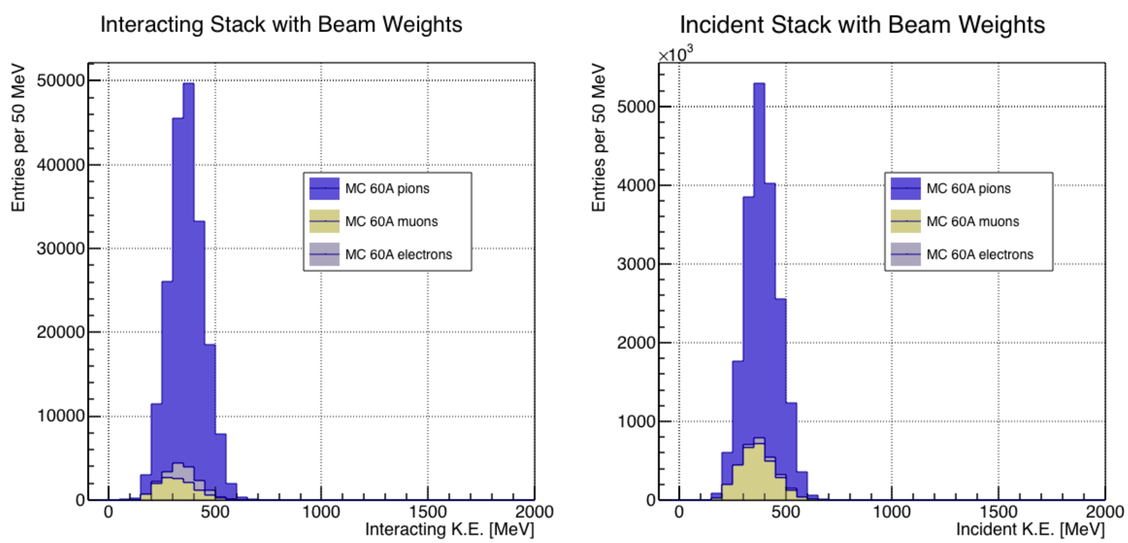


Figure 1.2: Left: staggered contributions to the interacting kinetic energy distribution for electron (grey), muons (yellow) and pion (blue) in the 60A simulation sample. Right: staggered contributions to the incident kinetic energy distribution for electron (grey), muons (yellow) and pion (blue) in the 60A simulation sample.

interacting and incident histograms separately. In data, we subtract this estimated relative contaminants contribution on the interacting and incident histograms bin by bin.

We estimate the systematic uncertainty on the cross section from this subtraction procedure by varying the electron to pion and muon to pion ratio in a suitable range of values. Figure

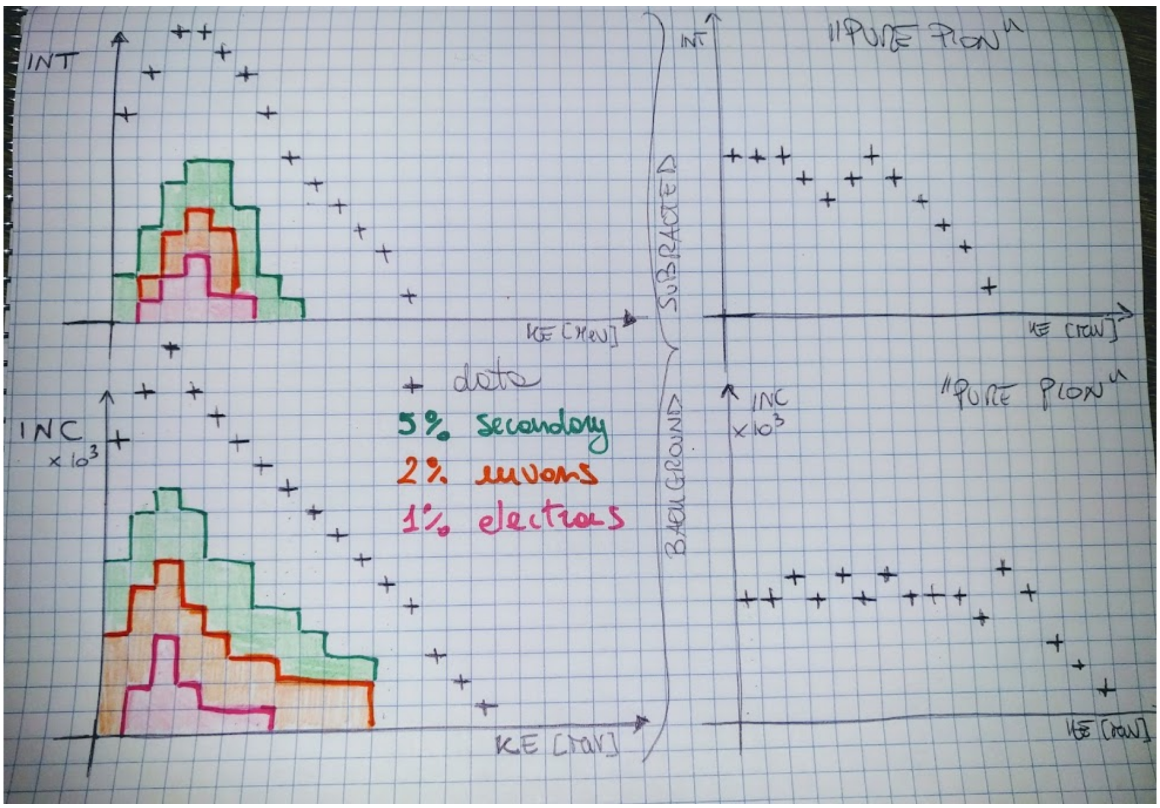


Figure 1.3: A graphical rendering of the beamline contamination background subtraction. The contribution of the contaminants is shown in green for the secondaries, in orange for the muons and in pink for electrons. The colored plots are coming from the MC and are staggered. The percentages shown in the legend are the percentages of contaminants over the total number of events passing the selection chain. We actually expect way less contamination.

## 1.3 Capture and decay

Our goal is to measure the total hadronic cross section for negative pions in argon. Since pion capture can be classified as an electromagnetic process and pion decay is a week process, capture and decay represent unwanted interactions. We present here a study of capture and decay in Monte Carlo and the solution we adopted to mitigate their present in the data sample.

For this MC study, we use a sample of 359000 MC pions generated according to the beam profile with the DDMC described in 0.2.2. It is important to notice that capture occurs predominantly at rest, while decay may occur both in flight and at rest. Thus, we can highly mitigate capture and decay at rest by removing pions which would release all their energy in the TPC and stop. This translates into a momentum selection, where we keep only events whose WC momentum is above a certain threshold. Figure 1.4 shows the true momentum distribution for the primary[2] pions that arrive to the TPC (pink), that capture (green) or decay (blue) inside the TPC, on a linear and log scale vertical axis.

In order to choose the selection value for the wire chamber momentum, it is beneficial to estimate the ratio of events which capture or decay that survive the selection in MC as a function of the momentum threshold, and compare it with the survival ratio for all events. This is done in figure 1.5. We define the survival ratio simply as the number of events surviving the true momentum selection divided by the number of events of that category. We calculate the survival ratio separately for the three event categories explained above: total (pink), capture (green) and decay (blue). Selecting pions with momentum greater than 420 MeV/c reduces the capture events by 99% while maintaining about 80% of the total data sample. Figure 1.6

2. We use here the Geant4 denomination "primary" to indicate that the pion considered does not undergo interactions modifying its energy before getting to the TPC. In fact, not every pion shot from wire chamber four will arrive to the TPC as primary, some will decay or interact before the TPC.

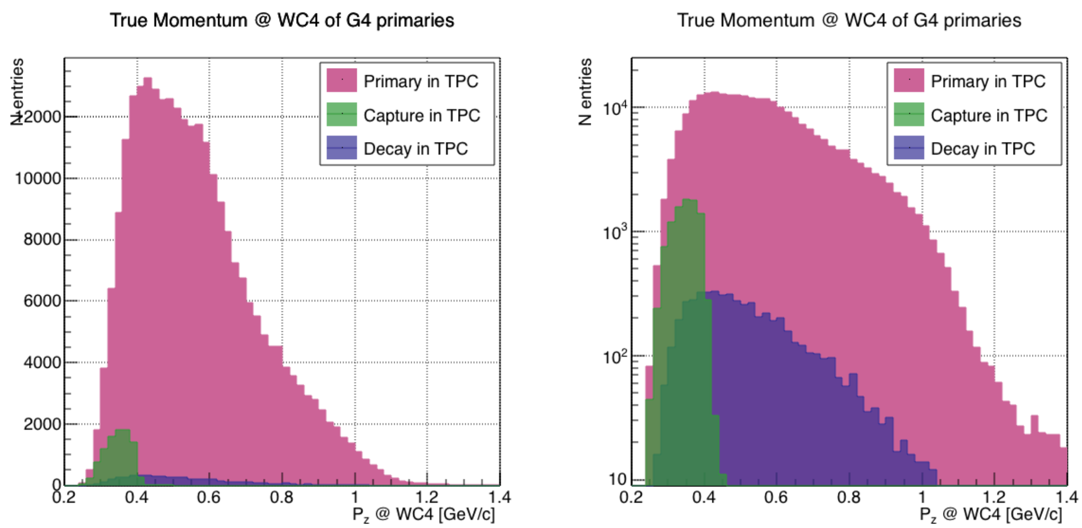


Figure 1.4: True momentum distribution at wire chamber 4 for every simulated pion arriving in the TPC (pink), ending its life in capture (green) or in decay (blue) in the TPC, linear vertical axis on the left, logarithmic on the right.

shows the ratio of events which end their life in capture (green) or decay (blue) over the total number of events as a as a function of the true momentum at wire chamber four. This ratio is slightly dependent on the inelastic cross section implemented in Geant4, as we are able to register a pion capture (or decay) only if it did not interact inelastically in the TPC. We choose a momentum threshold of 420 MeV/c because the percentage of capture events drops below 1% and the percentage of decays is never above 2% for momenta greater than 420 MeV/c.

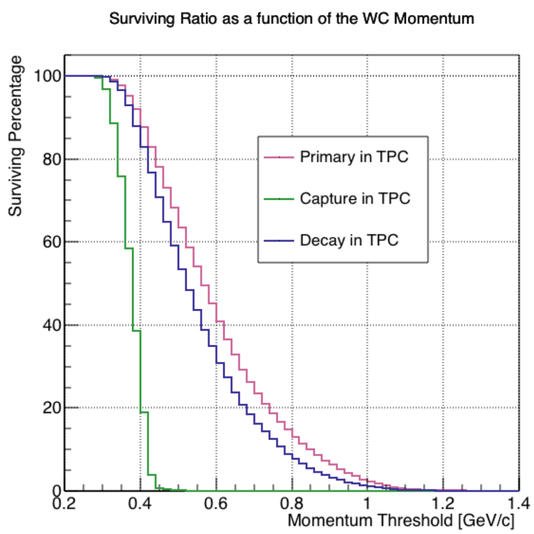


Figure 1.5: Survival ratio as a function of selection threshold on true momentum at wire chamber four for for every simulated pion arriving in the TPC (pink), capture (green) or in decay (blue).

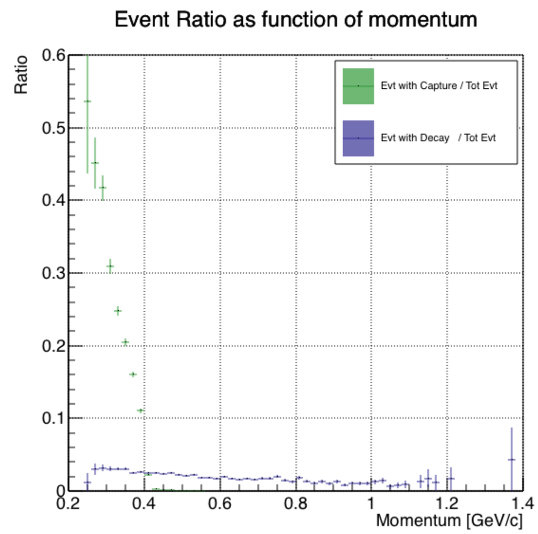


Figure 1.6: Ratio between the capture (green) and decay (blue) events over the total number of events as a as a function of the true momentum at wire chamber four.

# Bibliography

[1] Precision electroweak measurements on the z resonance. *Physics Reports*, 427(5):257 – 454, 2006.

[2] K. Abe, J. Amey, C. Andreopoulos, M. Antonova, S. Aoki, A. Ariga, D. Autiero, S. Ban, M. Barbi, G. J. Barker, G. Barr, C. Barry, P. Bartet-Friburg, M. Batkiewicz, V. Berardi, S. Berkman, S. Bhadra, S. Bienstock, A. Blondel, S. Bolognesi, S. Bordoni, S. B. Boyd, D. Brailsford, A. Bravar, C. Bronner, M. Buizza Avanzini, R. G. Calland, T. Campbell, S. Cao, S. L. Cartwright, M. G. Catanesi, A. Cervera, C. Checchia, D. Cherdack, N. Chikuma, G. Christodoulou, A. Clifton, J. Coleman, G. Collazuol, D. Coplowe, A. Cudd, A. Dabrowska, G. De Rosa, T. Dealtry, P. F. Denner, S. R. Dennis, C. Densham, D. Dewhurst, F. Di Lodovico, S. Di Luise, S. Dolan, O. Drapier, K. E. Duffy, J. Dumarchez, M. Dziewiecki, S. Emery-Schrenk, A. Ereditato, T. Feusels, A. J. Finch, G. A. Fiorentini, M. Friend, Y. Fujii, D. Fukuda, Y. Fukuda, V. Galymov, A. Garcia, C. Giganti, F. Gizzarelli, T. Golan, M. Gonin, D. R. Hadley, L. Haegel, M. D. Haigh, D. Hansen, J. Harada, M. Hartz, T. Hasegawa, N. C. Hastings, T. Hayashino, Y. Hayato, R. L. Helmer, A. Hillairet, T. Hiraki, A. Hiramoto, S. Hirota, M. Hogan, J. Holeczek, F. Hosomi, K. Huang, A. K. Ichikawa, M. Ikeda, J. Imber, J. Insler, R. A. Intonti, T. Ishida, T. Ishii, E. Iwai, K. Iwamoto, A. Izmaylov, B. Jamieson, M. Jiang, S. Johnson, P. Jonsson, C. K. Jung, M. Kabirnezhad, A. C. Kaboth, T. Kajita, H. Kakuno, J. Kameda,

D. Karlen, T. Katori, E. Kearns, M. Khabibullin, A. Khotjantsev, H. Kim, J. Kim, S. King, J. Kisiel, A. Knight, A. Knox, T. Kobayashi, L. Koch, T. Koga, A. Konaka, K. Kondo, L. L. Kormos, A. Korzenev, Y. Koshio, K. Kowalik, W. Kropp, Y. Kudenko, R. Kurjata, T. Kutter, J. Lagoda, I. Lamont, M. Lamoureux, E. Larkin, P. Lasorak, M. Laveder, M. Lawe, M. Licciardi, T. Lindner, Z. J. Liptak, R. P. Litchfield, X. Li, A. Longhin, J. P. Lopez, T. Lou, L. Ludovici, X. Lu, L. Magaletti, K. Mahn, M. Malek, S. Manly, A. D. Marino, J. F. Martin, P. Martins, S. Martynenko, T. Maruyama, V. Matveev, K. Mavrokoridis, W. Y. Ma, E. Mazzucato, M. McCarthy, N. McCauley, K. S. McFarland, C. McGrew, A. Mefodiev, C. Metelko, M. Mezzetto, P. Mijakowski, A. Minamino, O. Mineev, S. Mine, A. Missert, M. Miura, S. Moriyama, Th. A. Mueller, J. Myslik, T. Nakadaira, M. Nakahata, K. G. Nakamura, K. Nakamura, K. D. Nakamura, Y. Nakanishi, S. Nakayama, T. Nakaya, K. Nakayoshi, C. Nantais, C. Nielsen, M. Nirkko, K. Nishikawa, Y. Nishimura, P. Novella, J. Nowak, H. M. O'Keeffe, K. Okumura, T. Okusawa, W. Oryszczak, S. M. Oser, T. Ovsyannikova, R. A. Owen, Y. Oyama, V. Palladino, J. L. Palomino, V. Paolone, N. D. Patel, P. Paudyal, M. Pavin, D. Payne, J. D. Perkin, Y. Petrov, L. Pickard, L. Pickering, E. S. Pinzon Guerra, C. Pistillo, B. Popov, M. Posiadala-Zezula, J.-M. Poutissou, R. Poutissou, P. Przewlocki, B. Quilain, T. Radermacher, E. Radicioni, P. N. Ratoff, M. Ravonel, M. A. Rayner, A. Redij, E. Reinherz-Aronis, C. Riccio, P. A. Rodrigues, E. Rondio, B. Rossi, S. Roth, A. Rubbia, A. Rychter, K. Sakashita, F. Sánchez, E. Scantamburlo, K. Scholberg, J. Schwehr, M. Scott, Y. Seiya, T. Sekiguchi, H. Sekiya, D. Sgalaberna, R. Shah, A. Shaikhiev, F. Shaker, D. Shaw, M. Shiozawa, T. Shirahige, S. Short, M. Smy, J. T. Sobczyk, H. Sobel, M. Sorel, L. Southwell, J. Steinmann, T. Stewart, P. Stowell, Y. Suda, S. Suvorov, A. Suzuki, S. Y. Suzuki, Y. Suzuki, R. Tacik, M. Tada, A. Takeda, Y. Takeuchi, H. K. Tanaka, H. A. Tanaka, D. Terhorst, R. Terri,

T. Thakore, L. F. Thompson, S. Tobayama, W. Toki, T. Tomura, C. Touramanis, T. Tsukamoto, M. Tzanov, Y. Uchida, M. Vagins, Z. Vallari, G. Vasseur, T. Vladisavljevic, T. Wachala, C. W. Walter, D. Wark, M. O. Wascko, A. Weber, R. Wendell, R. J. Wilkes, M. J. Wilking, C. Wilkinson, J. R. Wilson, R. J. Wilson, C. Wret, Y. Yamada, K. Yamamoto, M. Yamamoto, C. Yanagisawa, T. Yano, S. Yen, N. Yershov, M. Yokoyama, K. Yoshida, T. Yuan, M. Yu, A. Zalewska, J. Zalipska, L. Zambelli, K. Zaremba, M. Ziembicki, E. D. Zimmerman, M. Zito, and J. Żmuda. Combined analysis of neutrino and antineutrino oscillations at t2k. *Phys. Rev. Lett.*, 118:151801, Apr 2017.

[3] R Acciarri, C Adams, J Asaadi, B Baller, T Bolton, C Bromberg, F Cavanna, E Church, D Edmunds, A Ereditato, S Farooq, B Fleming, H Greenlee, G Horton-Smith, C James, E Klein, K Lang, P Laurens, D McKee, R Mehdiyev, B Page, O Palamara, K Partyka, G Rameika, B Rebel, M Soderberg, J Spitz, A M Szelc, M Weber, M Wojcik, T Yang, and G P Zeller. A study of electron recombination using highly ionizing particles in the argoneut liquid argon tpc. *Journal of Instrumentation*, 8(08):P08005, 2013.

[4] R Acciarri, M Antonello, B Baibussinov, M Baldo-Ceolin, P Benetti, F Calaprice, E Calligarich, M Cambiaghi, N Canci, F Carbonara, F Cavanna, S Centro, A G Cocco, F Di Pompeo, G Fiorillo, C Galbiati, V Gallo, L Grandi, G Meng, I Modena, C Montanari, O Palamara, L Pandola, G B Piano Mortari, F Pietropaolo, G L Raselli, M Roncadelli, M Rossella, C Rubbia, E Segreto, A M Szelc, S Ventura, and C Vignoli. Effects of nitrogen contamination in liquid argon. *Journal of Instrumentation*, 5(06):P06003, 2010.

[5] R. Acciarri et al. Design and Construction of the MicroBooNE Detector. *JINST*, 12(02):P02017, 2017.

[6] R. Acciarri et al. First Observation of Low Energy Electron Neutrinos in a Liquid Argon Time Projection Chamber. *Phys. Rev.*, D95(7):072005, 2017. [Phys. Rev.D95,072005(2017)].

[7] M Adamowski, B Carls, E Dvorak, A Hahn, W Jaskierny, C Johnson, H Jostlein, C Kendziora, S Lockwitz, B Pahlka, R Plunkett, S Pordes, B Rebel, R Schmitt, M Stancari, T Tope, E Voirin, and T Yang. The liquid argon purity demonstrator. *Journal of Instrumentation*, 9(07):P07005, 2014.

[8] C. Adams et al. The Long-Baseline Neutrino Experiment: Exploring Fundamental Symmetries of the Universe. 2013.

[9] P. Adamson, L. Aliaga, D. Ambrose, N. Anfimov, A. Antoshkin, E. Arrieta-Diaz, K. Augsten, A. Aurisano, C. Backhouse, M. Baird, B. A. Bambah, K. Bays, B. Behera, S. Bending, R. Bernstein, V. Bhatnagar, B. Bhuyan, J. Bian, T. Blackburn, A. Bolshakova, C. Bromberg, J. Brown, G. Brunetti, N. Buchanan, A. Butkevich, V. Bychkov, M. Campbell, E. Catano-Mur, S. Childress, B. C. Choudhary, B. Chowdhury, T. E. Coan, J. A. B. Coelho, M. Colo, J. Cooper, L. Corwin, L. Cremonesi, D. Cronin-Hennessy, G. S. Davies, J. P. Davies, P. F. Derwent, R. Dharmapalan, P. Ding, Z. Djurcic, E. C. Dukes, H. Duyang, S. Edayath, R. Ehrlich, G. J. Feldman, M. J. Frank, M. Gabrielyan, H. R. Gallagher, S. Germani, T. Ghosh, A. Giri, R. A. Gomes, M. C. Goodman, V. Grichine, R. Group, D. Grover, B. Guo, A. Habig, J. Hartnell, R. Hatcher, A. Hatzikoutelis, K. Heller, A. Himmel, A. Holin, J. Hylen, F. Jediny, M. Judah, G. K. Kafka, D. Kalra, S. M. S. Kasahara, S. Kasetti, R. Keloth, L. Kolupaeva, S. Kotelnikov, I. Kourbanis, A. Kreymer, A. Kumar, S. Kurbanov, K. Lang, W. M. Lee, S. Lin, J. Liu, M. Lokajicek, J. Lozier, S. Luchuk, K. Maan, S. Magill, W. A. Mann, M. L. Marshak, K. Matera, V. Matveev, D. P. Méndez, M. D. Messier, H. Meyer, T. Miao, W. H. Miller, S. R. Mishra, R. Mohanta, A. Moren,

L. Mualem, M. Muether, S. Mufson, R. Murphy, J. Musser, J. K. Nelson, R. Nichol, E. Niner, A. Norman, T. Nosek, Y. Oksuzian, A. Olshevskiy, T. Olson, J. Paley, P. Pandey, R. B. Patterson, G. Pawloski, D. Pershey, O. Petrova, R. Petti, S. Phan-Budd, R. K. Plunkett, R. Poling, B. Potukuchi, C. Principato, F. Psihas, A. Radovic, R. A. Rameika, B. Rebel, B. Reed, D. Rocco, P. Rojas, V. Ryabov, K. Sachdev, P. Sail, O. Samoylov, M. C. Sanchez, R. Schroeter, J. Sepulveda-Quiroz, P. Shanahan, A. Sheshukov, J. Singh, J. Singh, P. Singh, V. Singh, J. Smolik, N. Solomey, E. Song, A. Sousa, K. Soustruznik, M. Strait, L. Suter, R. L. Talaga, M. C. Tamsett, P. Tas, R. B. Thayyullathil, J. Thomas, X. Tian, S. C. Tognini, J. Tripathi, A. Tsaris, J. Urheim, P. Vahle, J. Vasel, L. Vinton, A. Vold, T. Vrba, B. Wang, M. Wetstein, D. Whittington, S. G. Wojcicki, J. Wolcott, N. Yadav, S. Yang, J. Zalesak, B. Zamorano, and R. Zwaska. Constraints on oscillation parameters from $\nu_e$ appearance and $\nu_\mu$ disappearance in nova. *Phys. Rev. Lett.*, 118:231801, Jun 2017.

[10] A. Aguilar-Arevalo et al. Evidence for neutrino oscillations from the observation of anti-neutrino(electron) appearance in a anti-neutrino(muon) beam. *Phys. Rev.*, D64:112007, 2001.

[11] A. A. Aguilar-Arevalo et al. Improved Search for $\bar{\nu}_\mu \to \bar{\nu}_e$ Oscillations in the MiniBooNE Experiment. *Phys. Rev. Lett.*, 110:161801, 2013.

[12] S. Amoruso et al. Study of electron recombination in liquid argon with the ICARUS TPC. *Nucl. Instrum. Meth.*, A523:275–286, 2004.

[13] C. Anderson et al. The ArgoNeuT Detector in the NuMI Low-Energy beam line at Fermilab. *JINST*, 7:P10019, 2012.

[14] C. Andreopoulos et al. The GENIE Neutrino Monte Carlo Generator. *Nucl. Instrum. Meth.*, A614:87–104, 2010.

[15] M. Antonello, B. Baibussinov, P. Benetti, E. Calligarich, N. Canci, S. Centro, A. Cesana, K. Cieslik, D. B. Cline, A. G. Cocco, A. Dabrowska, D. Dequal, A. Dermenev, R. Dolfini, C. Farnese, A. Fava, A. Ferrari, G. Fiorillo, D. Gibin, S. Gninenko, A. Guglielmi, M. Haranczyk, J. Holeczek, A. Ivashkin, J. Kisiel, I. Kochanek, J. Lagoda, S. Mania, A. Menegolli, G. Meng, C. Montanari, S. Otwinowski, A. Piazzoli, P. Picchi, F. Pietropaolo, P. Plonski, A. Rappoldi, G. L. Raselli, M. Rossella, C. Rubbia, P. Sala, A. Scaramelli, E. Segreto, F. Sergiampietri, D. Stefan, J. Stepaniak, R. Sulej, M. Szarska, M. Terrani, F. Varanini, S. Ventura, C. Vignoli, H. Wang, X. Yang, A. Zalewska, and K. Zaremba. Precise 3d track reconstruction algorithm for the ICARUS t600 liquid argon time projection chamber detector. *Advances in High Energy Physics*, 2013:1–16, 2013.

[16] M. Antonello et al. A Proposal for a Three Detector Short-Baseline Neutrino Oscillation Program in the Fermilab Booster Neutrino Beam. 2015.

[17] D. Ashery, I. Navon, G. Azuelos, H. K. Walter, H. J. Pfeiffer, and F. W. Schlepütz. True absorption and scattering of pions on nuclei. *Phys. Rev. C*, 23:2173–2185, May 1981.

[18] C. Athanassopoulos et al. Evidence for nu(mu) → nu(e) neutrino oscillations from LSND. *Phys. Rev. Lett.*, 81:1774–1777, 1998.

[19] Borut Bajc, Junji Hisano, Takumi Kuwahara, and Yuji Omura. Threshold corrections to dimension-six proton decay operators in non-minimal {SUSY} su(5) {GUTs}. *Nuclear Physics B*, 910:1 – 22, 2016.

[20] B. Baller. Trajcluster user guide. Technical report, apr 2016.

[21] Gary Barker. Neutrino event reconstruction in a liquid argon TPC. *Journal of Physics: Conference Series*, 308:012015, jul 2011.

[22] J B Birks. Scintillations from organic crystals: Specific fluorescence and relative response to different radiations. *Proceedings of the Physical Society. Section A*, 64(10):874, 1951.

[23] A. Bodek and J. L. Ritchie. Further studies of fermi-motion effects in lepton scattering from nuclear targets. *Phys. Rev. D*, 24:1400–1402, Sep 1981.

[24] Mark G. Boulay and A. Hime. Direct WIMP detection using scintillation time discrimination in liquid argon. 2004.

[25] D. V. Bugg, R. S. Gilmore, K. M. Knight, D. C. Salter, G. H. Stafford, E. J. N. Wilson, J. D. Davies, J. D. Dowell, P. M. Hattersley, R. J. Homer, A. W. O'dell, A. A. Carter, R. J. Tapper, and K. F. Riley. Kaon-nucleon total cross sections from 0.6 to 2.65 gev/ $c$. *Phys. Rev.*, 168:1466–1475, Apr 1968.

[26] W. M. Burton and B. A. Powell. Fluorescence of tetraphenyl-butadiene in the vacuum ultraviolet. *Applied Optics*, 12(1):87, jan 1973.

[27] A. S. Carroll, I. H. Chiang, C. B. Dover, T. F. Kycia, K. K. Li, P. O. Mazur, D. N. Michael, P. M. Mockett, D. C. Rahm, and R. Rubinstein. Pion-nucleus total cross sections in the (3,3) resonance region. *Phys. Rev. C*, 14:635–638, Aug 1976.

[28] D. Casper. The nuance neutrino physics simulation, and the future. *Nuclear Physics B - Proceedings Supplements*, 112(1-3):161–170, nov 2002.

[29] A. Cervera, A. Donini, M.B. Gavela, J.J. Gomez Cádenas, P. Hernández, O. Mena, and S. Rigolin. Golden measurements at a neutrino factory. *Nuclear Physics B*, 579(1-2):17–55, jul 2000.

[30] E. Church. LArSoft: A Software Package for Liquid Argon Time Projection Drift Chambers. 2013.

[31] ATLAS Collaboration. Observation of a new particle in the search for the standard model higgs boson with the ATLAS detector at the LHC. *Physics Letters B*, 716(1):1–29, sep 2012.

[32] CMS Collaboration. Observation of a new boson at a mass of 125 gev with the cms experiment at the lhc. *Physics Letters B*, 716(1):30 – 61, 2012.

[33] The LArIAT Collaboration. The liquid argon in a testbeam (lariat) experiment. Technical report, In Preparation 2018.

[34] Stefano Dell'Oro, Simone Marcocci, Matteo Viel, and Francesco Vissani. Neutrinoless double beta decay: 2015 review. *Advances in High Energy Physics*, 2016:1–37, 2016.

[35] S.E. Derenzo, A.R. Kirschbaum, P.H. Eberhard, R.R. Ross, and F.T. Solmitz. Test of a liquid argon chamber with 20 m rms resolution. *Nuclear Instruments and Methods*, 122:319 – 327, 1974.

[36] Savas Dimopoulos, Stuart Raby, and Frank Wilczek. Proton Decay in Supersymmetric Models. *Phys. Lett.*, B112:133, 1982.

[37] D. Drakoulakos et al. Proposal to perform a high-statistics neutrino scattering experiment using a fine-grained detector in the NuMI beam. 2004.

[38] A Ereditato, C C Hsu, S Janos, I Kreslo, M Messina, C Rudolf von Rohr, B Rossi, T Strauss, M S Weber, and M Zeller. Design and operation of argontube: a 5 m long drift liquid argon tpc. *Journal of Instrumentation*, 8(07):P07002, 2013.

[39] Torleif Ericson and Wolfram Weise. *Pions and Nuclei (The International Series of Monographs on Physics)*. Oxford University Press, 1988.

[40] A.A. Aguilar-Arevalo et al. The miniboone detector. *Nuclear Instruments and Methods in Physics Research Section A: Accelerators, Spectrometers, Detectors and Associated Equipment*, 599(1):28 – 46, 2009.

[41] Antonio Bueno et al. Nucleon decay searches with large liquid argon TPC detectors at shallow depths: atmospheric neutrinos and cosmogenic backgrounds. *Journal of High Energy Physics*, 2007(04):041–041, apr 2007.

[42] A.S. Clough et al. Pion-nucleus total cross sections from 88 to 860 MeV. *Nuclear Physics B*, 76(1):15–28, jul 1974.

[43] B.W. Allardyce et al. Pion reaction cross sections and nuclear sizes. *Nuclear Physics A*, 209(1):1 – 51, 1973.

[44] C Athanassopoulos et al. The liquid scintillator neutrino detector and LAMPF neutrino source. *Nuclear Instruments and Methods in Physics Research Section A: Accelerators, Spectrometers, Detectors and Associated Equipment*, 388(1-2):149–172, mar 1997.

[45] F. Binon et al. Scattering of negative pions on carbon. *Nuclear Physics B*, 17(1):168 – 188, 1970.

[46] P. Vilain et al. Coherent single charged pion production by neutrinos. *Physics Letters B*, 313(1-2):267–275, aug 1993.

[47] R. Acciarri et al. Convolutional neural networks applied to neutrino events in a liquid argon time projection chamber. *Journal of Instrumentation*, 12(03):P03011, 2017.

[48] R. Acciarri et al. Design and construction of the MicroBooNE detector. *Journal of Instrumentation*, 12(02):P02017–P02017, feb 2017.

[49] C. E. Aalseth et al.l. DarkSide-20k: A 20 tonne two-phase LAr TPC for direct dark matter detection at LNGS. *The European Physical Journal Plus*, 133(3), mar 2018.

[50] H Fesbach. Theoretical nuclear physics: Nuclear reactions. 1992.

[51] J. A. Formaggio and G. P. Zeller. From ev to eev: Neutrino cross sections across energy scales. *Rev. Mod. Phys.*, 84:1307–1341, Sep 2012.

[52] E. Friedman et al. K+ nucleus reaction and total cross-sections: New analysis of transmission experiments. *Phys. Rev.*, C55:1304–1311, 1997.

[53] V.M. Gehman, S.R. Seibert, K. Rielage, A. Hime, Y. Sun, D.-M. Mei, J. Maassen, and D. Moore. Fluorescence efficiency and visible re-emission spectrum of tetraphenyl butadiene films at extreme ultraviolet wavelengths. *Nuclear Instruments and Methods in Physics Research Section A: Accelerators, Spectrometers, Detectors and Associated Equipment*, 654(1):116 – 121, 2011.

[54] Howard Georgi and S. L. Glashow. Unity of all elementary-particle forces. *Phys. Rev. Lett.*, 32:438–441, Feb 1974.

[55] D.Y. Wong (editor) G.L. Shaw (Editor). *Pion-nucleon Scattering*. John Wiley & Sons Inc, 1969.

[56] D S Gorbunov. Sterile neutrinos and their role in particle physics and cosmology. *Physics-Uspekhi*, 57(5):503, 2014.

[57] C. Green, J. Kowalkowski, M. Paterno, M. Fischler, L. Garren, and Q. Lu. The Art Framework. *J. Phys. Conf. Ser.*, 396:022020, 2012.

[58] J. Harada. Non-maximal $\boldsymbol{\theta_{23}}$ , large $\boldsymbol{\theta_{13}}$ and tri-bimaximal $\boldsymbol{\theta_{12}}$ via quark-lepton complementarity at next-to-leading order. *EPL (Europhysics Letters)*, 103(2):21001, 2013.

[59] Peter W. Higgs. Broken symmetries and the masses of gauge bosons. *Physical Review Letters*, 13(16):508–509, oct 1964.

[60] P.W. Higgs. Broken symmetries, massless particles and gauge fields. *Physics Letters*, 12(2):132–133, sep 1964.

[61] H J Hilke. Time projection chambers. *Reports on Progress in Physics*, 73(11):116201, 2010.

[62] N. Ishida, M. Chen, T. Doke, K. Hasuike, A. Hitachi, M. Gaudreau, M. Kase, Y. Kawada, J. Kikuchi, T. Komiyama, K. Kuwahara, K. Masuda, H. Okada, Y.H. Qu, M. Suzuki, and T. Takahashi. Attenuation length measurements of scintillation light in liquid rare gases and their mixtures using an improved reflection suppresser. *Nuclear Instruments and Methods in Physics Research Section A: Accelerators, Spectrometers, Detectors and Associated Equipment*, 384(2-3):380–386, jan 1997.

[63] George Jaffé. Zur theorie der ionisation in kolonnen. *Annalen der Physik*, 347(12):303–344, 1913.

[64] C. Jarlskog. A basis independent formulation of the connection between quark mass matrices, CP violation and experiment. *Zeitschrift für Physik C Particles and Fields*, 29(3):491–497, sep 1985.

[65] B J P Jones, C S Chiu, J M Conrad, C M Ignarra, T Katori, and M Toups. A measurement of the absorption of liquid argon scintillation light by dissolved nitrogen at the part-per-million level. *Journal of Instrumentation*, 8(07):P07011, 2013.

[66] Benjamin J. P. Jones. *Sterile Neutrinos in Cold Climates*. PhD thesis, MIT, 2015.

[67] Cezary Juszczak, Jarosław A. Nowak, and Jan T. Sobczyk. Simulations from a new neutrino event generator. *Nuclear Physics B - Proceedings Supplements*, 159:211–216, sep 2006.

[68] D. I. Kazakov. Beyond the standard model: In search of supersymmetry. In *2000 European School of high-energy physics, Caramulo, Portugal, 20 Aug-2 Sep 2000: Proceedings*, pages 125–199, 2000.

[69] Dae-Gyu Lee, R. N. Mohapatra, M. K. Parida, and Merostar Rani. Predictions for the proton lifetime in minimal nonsupersymmetric so(10) models: An update. *Phys. Rev. D*, 51:229–235, Jan 1995.

[70] M A Leigui de Oliveira. Expression of Interest for a Full-Scale Detector Engineering Test and Test Beam Calibration of a Single-Phase LAr TPC. Technical Report CERN-SPSC-2014-027. SPSC-EOI-011, CERN, Geneva, Oct 2014.

[71] W. H. Lippincott, K. J. Coakley, D. Gastler, A. Hime, E. Kearns, D. N. McKinsey, J. A. Nikkel, and L. C. Stonehill. Scintillation time dependence and pulse shape discrimination in liquid argon. *Phys. Rev. C*, 78:035801, Sep 2008.

[72] Jorge L. Lopez and Dimitri V. Nanopoulos. Flipped SU(5): Origins and recent developments. In *15th Johns Hopkins Workshop on Current Problems in Particle Theory: Particle Physics from Underground to Heaven Baltimore, Maryland, August 26-28, 1991*, pages 277–297, 1991.

[73] Vincent Lucas and Stuart Raby. Nucleon decay in a realistic so(10) susy gut. *Phys. Rev. D*, 55:6986–7009, Jun 1997.

[74] Ettore Majorana. Teoria simmetrica dell'elettrone e del positrone. *Il Nuovo Cimento*, 14(4):171–184, apr 1937.

[75] Hisakazu Minakata and Alexei Yu. Smirnov. Neutrino mixing and quark-lepton complementarity. *Phys. Rev. D*, 70:073009, Oct 2004.

[76] M. Mooney. The microboone experiment and the impact of space charge effects. 2015.

[77] E. Morikawa, R. Reininger, P. Gürtler, V. Saile, and P. Laporte. Argon, krypton, and xenon excimer luminescence: From the dilute gas to the condensed phase. *The Journal of Chemical Physics*, 91(3):1469–1477, aug 1989.

[78] Emmy Noether. Invariant variation problems. *Transport Theory and Statistical Physics*, 1(3):186–207, jan 1971.

[79] I. Nutini. Study of charged particles interaction processes on ar in the 0.2 - 2.0 GeV energy range through combined information from ionization free charge and scintillation light. Technical report, jan 2015.

[80] D. R. Nygren. The time projection chamber: A new 4 $\pi$ detector for charged particles. Technical report, 1974.

[81] L. Onsager. Initial recombination of ions. *Phys. Rev.*, 54:554–557, Oct 1938.

[82] S. Pascoli, S.T. Petcov, and A. Riotto. Leptogenesis and low energy cp-violation in neutrino physics. *Nuclear Physics B*, 774(1):1 – 52, 2007.

[83] C. Patrignani et al. Review of Particle Physics. *Chin. Phys.*, C40(10):100001, 2016.

[84] B. Pontecorvo. Neutrino Experiments and the Problem of Conservation of Leptonic Charge. *Sov. Phys. JETP*, 26:984–988, 1968. [Zh. Eksp. Teor. Fiz.53,1717(1967)].

[85] T. Yang R. Acciarri, M. Stancari. Determination of the electron lifetime in lariat. Technical report, March 2016.

[86] Martti Raidal. Relation between the neutrino and quark mixing angles and grand unification. *Phys. Rev. Lett.*, 93:161801, Oct 2004.

[87] Steve Ritz et al. Building for Discovery: Strategic Plan for U.S. Particle Physics in the Global Context. 2014.

[88] C. Rubbia. The Liquid Argon Time Projection Chamber: A New Concept for Neutrino Detectors. 1977.

[89] L.M. Saunders. Electromagnetic production of pions from nuclei. *Nucl. Phys., B7: 293-310(1968).*

[90] Qaisar Shafi and Zurab Tavartkiladze. Neutrino democracy, fermion mass hierarchies, and proton decay from 5d su(5). *Phys. Rev. D*, 67:075007, Apr 2003.

[91] R. K. Teague and C. J. Pings. Refractive index and the lorentz–lorenz function for gaseous and liquid argon, including a study of the coexistence curve near the critical state. *The Journal of Chemical Physics*, 48(11):4973–4984, jun 1968.

[92] J. Thomas and D. A. Imel. Recombination of electron-ion pairs in liquid argon and liquid xenon. *Phys. Rev. A*, 36:614–616, Jul 1987.

[93] D.R.O. Morrison N. Rivoire V. Flaminio, W.G. Moorhead. Compilation of Cross Sections I: $\pi^+$ and $\pi^-$ Induced Reactions. *CERN-HERA*, pages 83–01, 1983.

[94] D.R.O. Morrison N. Rivoire V. Flaminio, W.G. Moorhead. Compilation of Cross Sections II: $K^+$ and $K^-$ Induced Reactions. *CERN-HERA*, pages 83–02, 1983.

[95] Hermann Weyl. Gravitation and the electron. *Proceedings of the National Academy of Sciences of the United States of America*, 15(4):323–334, 1929.

[96] Colin et al Wilkin. A comparison of pi+ and pi- total cross-sections of light nuclei near the 3-3 resonance. *Nucl. Phys.*, B62:61–85, 1973.

[97] D. H. Wright and M. H. Kelsey. The Geant4 Bertini Cascade. *Nucl. Instrum. Meth.*, A804:175–188, 2015.

[98] C. S. Wu, E. Ambler, R. W. Hayward, D. D. Hoppes, and R. P. Hudson. Experimental test of parity conservation in beta decay. *Phys. Rev.*, 105:1413–1415, Feb 1957.

[99] N Yahlali, L M P Fernandes, K Gonzlez, A N C Garcia, and A Soriano. Imaging with sipms in noble-gas detectors. *Journal of Instrumentation*, 8(01):C01003, 2013.

[100] T. Yanagida. Horizontal symmetry and masses of neutrinos. *Progress of Theoretical Physics*, 64(3):1103–1105, sep 1980.